Research Article | Vol. 29, No. 18 / 30 Aug 2021 / Optics Express 28778
Optics EXPRESS

Thermal tuning of a fiber-integrated Fabry-Pérot cavity

CLEMENS SINGER,[1,3] ALEXANDER GOETZ,[1,3] ADARSH S. PRASAD,[1] MARTIN BECKER,[2] MANFRED ROTHHARDT,[2] AND SARAH M. SKOFF[1,*]

[1] *Vienna Center for Quantum Science and Technology, Atominstitut, Technische Universität Wien, Stadionallee 2, 1020 Vienna, Austria*
[2] *Leibniz Institute of Photonic Technology, Albert-Einstein-Strasse 9, 07745 Jena, Germany*
[3] *Co-first authors with equal contribution*
[*] *sarah.skoff@tuwien.ac.at*

Abstract: Here, we present the thermal tuning capability of an alignment-free, fiber-integrated Fabry-Pérot cavity. The two mirrors are made of fiber Bragg gratings that can be individually temperature stabilized and tuned. We show the temperature tuning of the resonance wavelength of the cavity without any degradation of the finesse and the tuning of the individual stop bands of the fiber Bragg gratings. This not only permits for the cavity's finesse to be optimized post-fabrication but also makes this cavity applicable as a narrowband filter with a FWHM spectral width of 0.07 ± 0.02 pm and a suppression of more than -15 dB that can be wavelength tuned. Further, in the field of quantum optics, where strong light-matter interactions are desirable, quantum emitters can be coupled to such a cavity and the cavity effect can be reversibly omitted and re-established. This is particularly useful when working with solid-state quantum emitters where such a reference measurement is often not possible once an emitter has been permanently deposited inside a cavity.

1. Introduction

Fiber Bragg gratings are used for a variety of technological applications due to their small size, their compatibility with optical fibers which naturally comes with an ease in signal transmission and their ability for multiplexing. They have been used as temperature [1], refractive index [2–4], strain [5], magnetic fields [6] and pressure sensors [7,8] and for measurements of windspeed, liquid levels, liquid density and specific gravity [9]. By using two gratings to form a Fabry-Pérot cavity they have also shown the potential to function as narrowband filters [10,11]. Their suitability for forming an alignment-free Fabry-Pérot type cavity [12] has also opened up their application in the field of quantum optics, where the fiber connecting two such fiber Bragg gratings can be readily tapered to guide the light between the gratings as an evanescent wave [13–16]. This allows for efficient coupling of quantum emitters to the guided light field of such nanofiber-based cavities. For all these applications, a tunability of the fiber Bragg gratings is desirable especially when it is required to match the resonance of a specific quantum emitter or transmit or reflect light in a narrow wavelength range [17]. For that purpose, complex designs exist to electrically tune a fiber Bragg grating cavity [10]. Here, we demonstrate the thermal tunability of a fiber Bragg grating Fabry-Pérot cavity, where each fiber Bragg grating can be individually temperature stabilized and tuned. This simple design not only enables to find the perfect overlap of the stop bands of the individual fiber Bragg gratings and thus highest finesse of the cavity post-fabrication but also allows for tuning the stop band of the two fiber Bragg gratings far enough such that the cavity effect can be reversibly suspended and re-established. This is particularly useful for coupling solid-state quantum emitters to such cavities as it allows for reference measurements with and without a cavity structure which is otherwise often not

#433094 https://doi.org/10.1364/OE.433094
Journal © 2021 Received 3 Jun 2021; revised 23 Jul 2021; accepted 6 Aug 2021; published 23 Aug 2021

Optics EXPRESS

possible once an emitter is permanently deposited in a cavity. In addition it finds its applicability in quantum optics to separate probe and control fields that are often narrowband and may be only separated by a few GHz [17,18]. This in-fiber cavity therefore conveniently allows the suppression of one beam compared to the other by more than -15dB which can be easily increased by concatenating such in-fiber cavities without the need for alignment.

2. Experimental setup

The Fabry-Pérot cavity is written into a commercial single mode fiber (SM600) by a pulsed 248 nm KrF laser that generates the two fiber Bragg gratings at a distance of 25 mm from each other [19]. 20 mm is about the minimum distance required if one wishes to taper the fiber between the mirrors later on, as the hydrogen-oxygen flame used during the heat and pull process needs to fit between the gratings without affecting their performance. If this cavity is used as a filter there exists no such restriction [20]. To be able to stabilize and temperature tune the two gratings individually, two PID controllers (Arroyo Instruments) are used in conjunction with two Peltier elements and two thermistors that cool or heat and monitor the temperature, respectively.

There are other heating techniques that can in principle be used, such as internal laser heating [7,11] or resistive heating via a thin metal coating around the fiber [21] but these methods do not allow for cooling of the fiber grating. In addition, the fiber Bragg gratings can also be tuned by strain but all these methods require more sophisticated set-ups [22]. In our case, the cavity holder (Fig. 1) consists of a U-shaped ground plate, made from aluminium, and two copper plates on top, that keep the Peltier elements and the fiber in place. The Peltier elements are fixed in the mount by grooves, just deep enough for the elements to stay in place but not too deep, so that the top and bottom parts of the Peltier elements are not thermally coupled via the aluminium holder. The fiber is placed between the Peltier elements and copper plates. Copper in conjunction with thermal silicon grease was used to ensure an even distribution of heat across the whole length of the fiber beneath. The temperature sensors are then clamped on the top copper plates with two additional thin copper plates. This cavity is characterized by a widely tunable laser (New Focus TLB 6700) where the transmission is monitored by two photodiodes or single photon counting modules. Before the light enters the cavity it is passing through three polarization paddles, which can be tilted to adjust the polarization of the light. This is necessary to end up with only one resonant mode inside the cavity [14]. Before the beam enters the cavity some light is picked off to monitor the wavelength via a wavemeter which continuously monitors the laser frequency with a relative precision better than 3×10^{-7}.

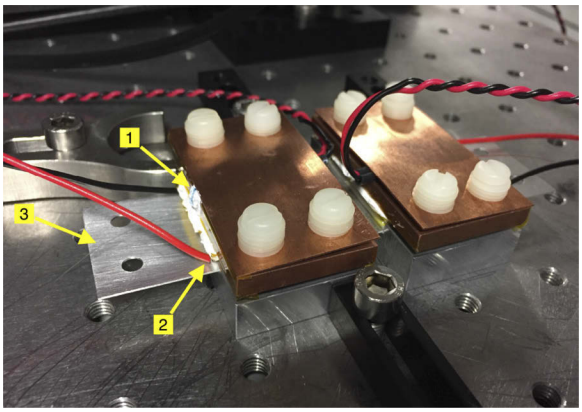

Fig. 1. Fiber mount with (1) the thermistor in the hole of the top plate, (2) the Peltier element on the bottom and (3) the fiber itself.

Optics EXPRESS

3. Results

3.1. Individually tuning the stop bands of the two fiber Bragg gratings

Although the Bragg gratings are manufactured for a particular Bragg wavelength λ_B given by $\lambda_B = 2n_{eff}\,\Lambda$, where Λ is the grating period and n_{eff} the effective refractive index, there might still be a slight mismatch between two gratings after manufacturing that results in a lower finesse than could be achieved. To maximise the overlap between the two gratings, one is held at a constant temperature of 22°C as the other grating is heated from 10°C to 60°C. Once there is an overlap between the two stopbands and a cavity effect can be observed, the finesse F is obtained by fitting an Airy function with constant offset d, free spectral range λ_{FSR} and transmission on resonance T_0:

$$T(\lambda) = d + \frac{T_0}{1 + \frac{4\mathcal{F}^2}{\pi^2}\sin^2\left(\frac{\pi(\lambda-\lambda_0)}{\lambda_{FSR}}\right)}, \tag{1}$$

to two spectral lines at a time. The highest finesse at a particular wavelength then indicates the wavelength of best overlap of the two stop bands at a particular temperature of the second grating [13]. The finesse is plotted as a function of grating temperature in Fig. 2. Each datapoint in Fig. 2 corresponds to the mean of three measurements and the error bars represent its standard deviation. It can be seen, that the highest finesse value and thus the best overlap of the two stopbands is reached, when grating one is heated to 40°C, where the finesse reaches 124 ± 15.

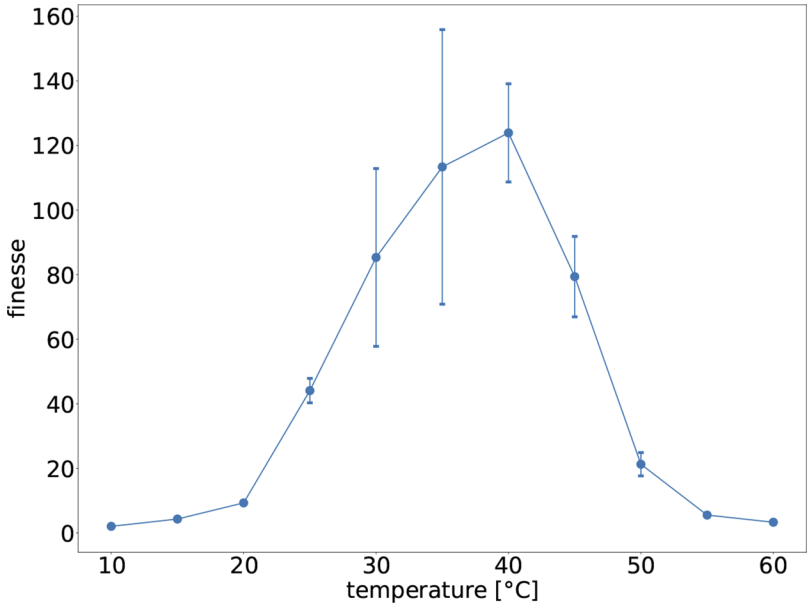

Fig. 2. Maximum finesse values (a) in transmission when grating one is heated from 10 to 60°C and grating two is constantly held at 22°C.

We are also able to detune the two gratings far enough so that the individual stop bands can be seen and the cavity effect is eliminated (Fig. 3(a)). Figure 3(b) shows the overlap with both gratings at room temperature and Fig. 3(c) shows the transmission spectrum of the cavity with an optimized overlap of the individual stopbands. In Fig. 3(d), a zoom in of the transmission peaks at best overlap as in c) is displayed including a fit to Eq. (1) and an inset which shows the transmission in dB to infer the possible suppression of unwanted light by this type of filter.

Optics EXPRESS

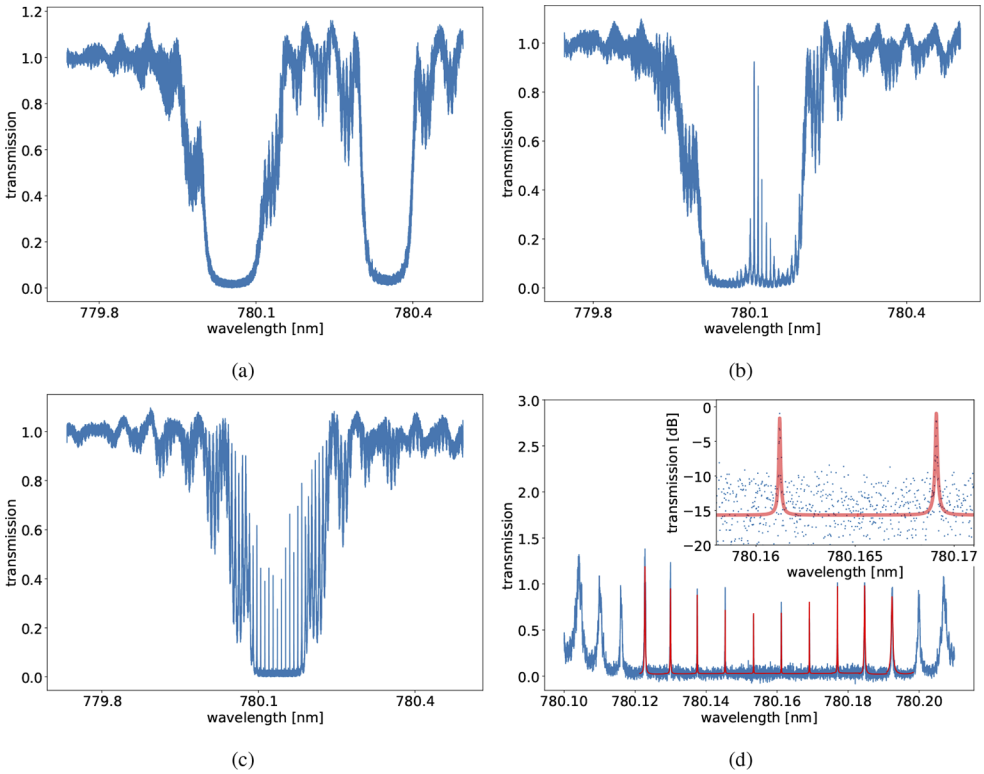

Fig. 3. Transmission spectra (a) showing two separate stop bands (grating 1 at 22°, grating 2 at 60°), with grating 1 and 2 at room temperature (b) showing the finesse that is obtained without any temperature tuning and (c) showing the best overlap (grating 1 at 37° and grating 2 at 22°). d) zoomed in region of transmission peaks at best overlap with an inset that shows the transmission plotted with a db scale to show functionality as a narrowband filter

3.2. *Tuning the center frequency of the cavity*

Whether such a cavity is used as a narrowband filter or to enhance the light-matter interaction between a light field and a quantum emitter, it may be necessary to tune the center frequency of the cavity. The Bragg wavelength λ_B of a Fiber-Bragg-Grating increases when the grating is heated. This effect originates from two sources. Firstly, thermal expansion of the fiber itself causes an increase of the distance between each grating and secondly the effective refractive index of the material n changes with temperature. Both these effects on the Bragg wavelength are described by the following equation,

$$\Delta\lambda_B = \lambda_B(\alpha_T + \alpha_n)\Delta T, \tag{2}$$

where α_T is the thermal expansion coefficient and α_n the thermo optic coefficient accounting for the change in effective refractive index. By tracking the position of narrow features in the reflection spectra, it is possible to obtain the wavelength shift of the two gratings as a function of temperature. It has been previously demonstrated that the temperature-dependent wavelength shift for a temperature range between 10-60 degrees is linear with temperature [8,23–25] and hence the resulting datapoints were fitted with a linear function [23] that showed a shift of 6.3 ± 0.3 pm/K for grating one and 5.0 ± 0.2 pm/K for grating two. These values are in agreement with the temperature-dependent wavelength shift of the Bragg grating in silica [8,23,25,26]. In principle this shift can be enhanced further by bonding the fiber to a substrate with a large thermal

Optics EXPRESS

expansion coefficient such as copper, in which case we would expect the shift to increase to 13.41 pm/K [27]. In our current set-up by just fixing the fiber loosely with some Kapton tape on the Peltier element, and then clamping it with the copper plate, as expected we see no influence of the surrounding material on the wavelength shift.

The measurements of the wavelength shift (Fig. 4), together with the known point of maximum overlap (Fig. 2) and hence largest finesse, makes it possible to temperature control both gratings in such a way that the overlap is kept at the optimum with an average finesse of 129 ± 11 across a tuning range of about 160 pm as depicted in Fig. 5.

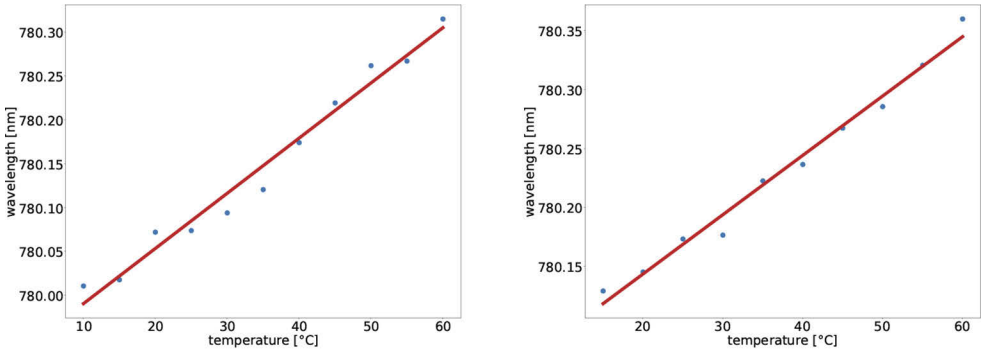

(a) Shift of grating one

(b) Shift of grating two

Fig. 4. Shift of grating one

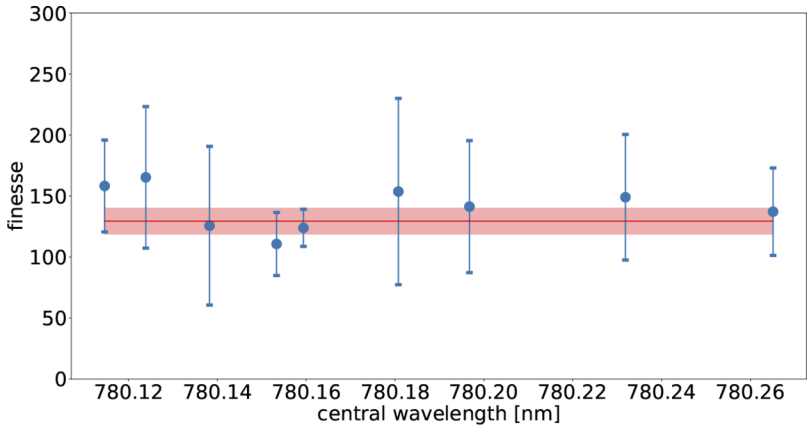

Fig. 5. Maximum finesse values as the center frequency of the cavity is temperature-tuned. The datapoints are the mean value of three measurements and the error bars are the corresponding standard deviation

4. Conclusion

In summary, we have demonstrated a fiber-integrated cavity that can be temperature tuned over hundreds of pm while keeping the good performance as other microcavites [28–34] show.This tuning allows for finding the best overlap between the two fiber Bragg gratings to optimise the finesse even after the gratings have been fabricated. The temperature control together with the finite width of the stop bands of the individual fiber Bragg gratings that function as the

Optics EXPRESS

mirrors of this Fabry-Pérot type cavity has further allowed us to reversibly and controllably omit and re-establish the cavity effect. This can be especially important when coupling solid-state quantum emitters to such cavities as can be readily done by placing an emitter on a tapered fiber section between the gratings [13], thereby creating a cavity that is able to reach the strong coupling regime. A Purcell factor of 15 has been shown to be achievable in this way with a mode volume of $4.9 \times 10^4\ \lambda^3$ and typical Q-factors of 10^7 [13]. These values were obtained for a taper transmission of 93% which can be improved further, as values of better than 99.95% have been demonstrated [35]. The tunability of such a cavity as demonstrated here then allows for convenient reference measurements with and without the cavity, something which is otherwise often not possible with permanently deposited solid-state quantum emitters. The tuning range of the cavity's center frequency without any degradation of the finesse allows coupling to solid-state emitters such as colour centers in diamond [36], single molecules in solids [37–39], or novel quantum emitters such as colour centers in 2D materials [40] or silicon carbide [41], that have an inherent inhomogeneous broading due to their nanoenvironment. Quantum emitters in 2D materials have recently shown Fourier-limited emission at room temperature [42,43] and colour centers in nanodiamonds were coupled to a cavity at room-temperature to observe a funneling effect of its initial broad emission [44]. If nevertheless cryogenic temperatures are required, the nanofiber section can in principal be cooled via contact gas to cryogenic temperatures while the fiber Bragg gratings can reside outside this cryogenic region. In the broader context of photonics, the demonstrated tunability of the individual stop bands further allows this cavity to function as a wavelength tunable narrowband filter that is alignment-free and can be easily incorporated in any experiment. Our results therefore promise a wide applicability of these fiber-integrated Bragg grating cavities not only in quantum optics [45,46] but also for new photonic technologies [47–49]

Appendix: behaviour of finesse as one grating is detuned

The finesse of the cavity is determined by the overlap of the two stop bands [50] of grating 1 and grating 2. As we can detune the gratings far enough to determine their individual stop bands (Fig. 3) and measure their temperature dependent wavelength shift (Fig. 4), the behaviour of finesse versus temperature can be estimated by inserting the reflectivities (R1, R2) of the stop bands into the equation for the finesse of a Fabry-Pérot cavity:

$$\mathcal{F} = \frac{\pi \sqrt[4]{R_1 R_2}}{1 - \sqrt{R_1 R_2}}. \tag{3}$$

To obtain the best finesse for each temperature, the finesse values are averaged over the wavelength range of one free-spectral range and the error displayed is the corresponding standard deviation. In Fig. 6, we compare these results with those obtained by directly evaluating the maximum finesse from the cavity fringes at different temperatures of the grating (Fig. 2) and show that they are in good agreement.

Optics EXPRESS

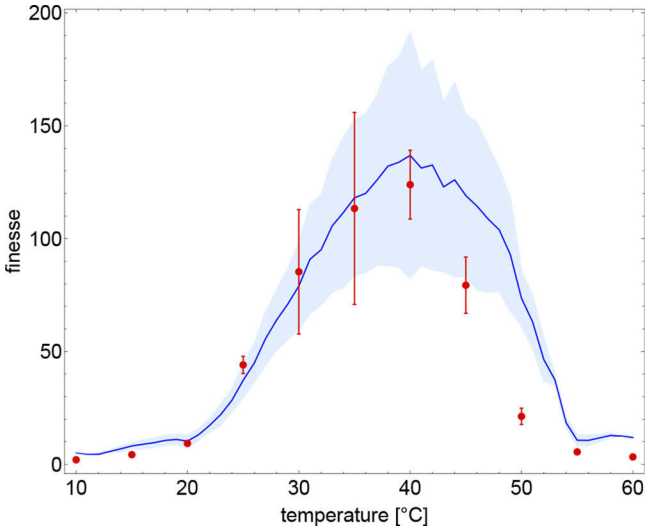

Fig. 6. Dependence of the finesse of the cavity as grating 1 is temperature-tuned and grating 2 is held at 22°C. The blue curve and corresponding error show the expected finesse evaluated from the individual stop bands of the two gratings that make up the cavity and the red data points are the results of the finesse obtained from directly fitting the cavity fringes at different temperatures of grating 1.

Funding. European Commission (800942); Österreichischen Akademie der Wissenschaften (1847108).

Acknowledgements. We want to thank Arno Rauschenbeutel for the loan of equipment.

Disclosures. The authors declare no conflicts of interest.

Data availability. Data underlying the results presented in this paper are not publicly available at this time but may be obtained from the authors upon reasonable request.

References

1. S. Tao, X. Dong, and B. Lai, "A Sensor for Simultaneous Measurement of Displacement and Temperature Based on the Fabry-Pérot Effect of a Fiber Bragg Grating," IEEE Sens. J. **17**(2), 261–266 (2017).
2. M. F. S. Ferreira, G. Statkiewicz-Barabach, D. Kowal, P. Mergo, W. Urbanczyk, and O. Fraz ao, "Fabry-Perot cavity based on polymer FBG as refractive index sensor," Opt. Commun. **394**, 37–40 (2017).
3. K. Zhou, Z. Yan, L. Zhang, and I. Bennion, "Refractometer based on fiber Bragg grating Fabry-Pérot cavity embedded with a narrow microchannel," Opt. Express **19**(12), 11769–11779 (2011).
4. C. Gouveia, P. A. S. Jorge, J. M. Baptista, and O. Frazao, "Fabry–Pérot Cavity Based on a High-Birefringent Fiber Bragg Grating for Refractive Index and Temperature Measurement," IEEE Sens. J. **12**(1), 17–21 (2012).
5. K. Markowski, K. Jędrzejewski, M. Marzęcki, and T. Osuch, "Linearly chirped tapered fiber-Bragg-grating-based Fabry-Perot cavity and its application in simultaneous strain and temperature measurement," Opt. Lett. **42**(7), 1464–1467 (2017).
6. Y. Zhao, R. Lv, D. Wang, and Q. Wang, "Fiber Optic Fabry-Perot Magnetic Field Sensor With Temperature Compensation Using a Fiber Bragg Grating," IEEE Trans. Instrum. Meas. **63**(9), 2210–2214 (2014).
7. S. Gao, A. P. Zhang, H.-Y. Tam, L. H. Cho, and C. Lu, "All-optical fiber anemometer based on laser heated fiber Bragg gratings," Opt. Express **19**(11), 10124–10130 (2011).
8. A. Othonos, "Fiber Bragg gratings," Rev. Sci. Instrum. **68**(12), 4309–4341 (1997).
9. C.-W. Lai, Y.-L. Lo, J.-P. Yur, W.-F. Liu, and C.-H. Chuang, "Application of Fabry–Pérot and fiber Bragg grating pressure sensors to simultaneous measurement of liquid level and specific gravity," Measurement **45**(3), 469–473 (2012).
10. W. Zhang, N. Ehteshami, W. Liu, and J. Yao, "Silicon-based on-chip electrically tunable sidewall Bragg grating Fabry-Perot filter," Opt. Lett. **40**(13), 3153–3156 (2015).
11. B. Zhou, H. Jiang, R. Wang, and C. Lu, "Optical Fiber Fiber Fabry–Perot Filter With Tunable Cavity for High-Precision Resonance Wavelength Adjustment," J. Lightwave Technol. **33**, 1 (2015).
12. F. Wei, F. Yang, X. Zhang, D. Xu, M. Ding, L. Zhang, D. Chen, H. Cai, Z. Fang, and G. Xijia, "Subkilohertz linewidth reduction of a DFB diode laser using self-injection locking with a fiber Bragg grating Fabry-Perot cavity," Opt. Express **24**(15), 17406–17415 (2016).

Optics EXPRESS

13. J. Hütner, T. Hoinkes, M. Becker, M. Rothhardt, A. Rauschenbeutel, and S. M. Skoff, "Nanofiber-based high-Q microresonator for cryogenic applications," Opt. Express **28**(3), 3249 (2020).
14. C. Wuttke, M. Becker, S. Brückner, M. Rothhardt, and A. Rauschenbeutel, "Nanofiber Fabry–Perot microresonator for nonlinear optics and cavity quantum electrodynamics," Opt. Lett. **37**(11), 1949–1951 (2012).
15. A. W. Schell, H. Takashima, S. Kamioka, Y. Oe, M. Fujiwara, O. Benson, and S. Takeuchi, "Highly Efficient Coupling of Nanolight Emitters to a Ultra-Wide Tunable Nanofibre Cavity," Sci. Rep. **5**(1), 9619 (2015).
16. S. Kato and T. Aoki, "Strong Coupling between a Trapped Single Atom and an All-Fiber Cavity," Phys. Rev. Lett. **115**(9), 093603 (2015).
17. J. P. Hedger, T. Elsmann, M. Becker, T. Tiess, A. N. Luiten, and B. M. Sparkes, "High Performance Fiber-Fabry-Perot Resonator Targeting Quantum Optics Applications," IEEE Photonics Technol. Lett. **32**(14), 879–882 (2020).
18. P. Burdekin, S. Grandi, R. Newbold, R. A. Hoggarth, K. D. Major, and A. S. Clark, "Single-photon-level sub-doppler pump-probe spectroscopy of rubidium," Phys. Rev. Appl. **14**(4), 044046 (2020).
19. E. Lindner, C. Chojetzki, S. Brückner, M. Becker, M. Rothhardt, and H. Bartelt, "Thermal regeneration of fiber Bragg gratings in photosensitive fibers," Opt. Express **17**(15), 12523–12531 (2009).
20. I. Petermann, B. Sahlgren, S. Helmfrid, A. T. Friberg, and P.-Y. Fonjallaz, "Fabrication of advanced fiber Bragg gratings by use of sequential writing with a continuous-wave ultraviolet laser source," Appl. Opt. **41**(6), 1051–1056 (2002).
21. J. A. Rogers, B. J. Eggleton, J. R. Pedrazzani, and T. A. Strasser, "Distributed on-fiber thin film heaters for Bragg gratings with adjustable chirp," Appl. Phys. Lett. **74**(21), 3131–3133 (1999).
22. S. Liu, X. Dong, J. Sun, and P. Shum, "Free-spectral range tunable Fabry–Perot filter with superimposed fiber Bragg gratings," Opt. Commun. **282**(24), 4729–4732 (2009).
23. M. B. Reid and M. Ozcan, "Temperature dependence of fiber optic Bragg gratings at low temperatures," Opt. Eng. **37**(1), 237–240 (1998).
24. K. Hill and G. Meltz, "Fiber Bragg grating technology- fundamentals and overview," J. Lightwave Technol. **15**(8), 1263–1276 (1997).
25. J. M. Jewell, "Thermooptic coefficients of some standard reference material glasses," J. Am. Ceram. Soc. **74**(7), 1689–1691 (1991).
26. W. P. Reed, "Standard reference material 739," https://www-s.nist.gov/srmors/certificates/archive/739.pdf.
27. F. R. Kroeger and C. A. Swenson, "Absolute linear thermal-expansion measurements on copper and aluminum from 5 to 320 k," J. Appl. Phys. **48**(3), 853–864 (1977).
28. A. Faraon, P. E. Barclay, C. Santori, K.-M. C. Fu, and R. G. Beausoleil, "Resonant enhancement of the zero-phonon emission from a colour centre in a diamond cavity," Nat. Photonics **5**(5), 301–305 (2011).
29. J. Gallego, W. Alt, T. Macha, M. Martinez-Dorantes, D. Pandey, and D. Meschede, "Strong Purcell effect on a neutral atom trapped in an open fiber cavity," arXiv:1804.08526 [physics, physics:quant-ph] (2018).
30. M. Fujiwara, T. Noda, A. Tanaka, K. Toubaru, H.-Q. Zhao, and S. Takeuchi, "Coupling of ultrathin tapered fibers with high-Q microsphere resonators at cryogenic temperatures and observation of phase-shift transition from undercoupling to overcoupling," Opt. Express **20**(17), 19545–19553 (2012).
31. T. Herzog, M. Sartison, S. Kolatschek, S. Hepp, A. Bommer, C. Pauly, F. Mücklich, C. Becher, M. Jetter, S. L. Portalupi, and P. Michler, "Pure single-photon emission from in(ga)as qds in a tunable fiber-based external mirror microcavity," Quantum Sci. Technol. **3**(3), 034009 (2018).
32. D. Wang, H. Kelkar, D. Martin-Cano, D. Rattenbacher, A. Shkarin, S. Utikal, T. Götzinger, and V. Sandoghdar, "Turning a molecule into a coherent two-level quantum system," Nat. Phys. **15**(5), 483–489 (2019).
33. R. Henze, J. M. Ward, and O. Benson, "Temperature independent tuning of whispering gallery modes in a cryogenic environment," Opt. Express **21**(1), 675–680 (2013).
34. D. Rattenbacher, A. Shkarin, J. Renger, T. Utikal, S. Götzinger, and V. Sandoghdar, "Coherent coupling of single molecules to on-chip ring resonators," New J. Phys. **21**(6), 062002 (2019).
35. J. E. Hoffman, S. Ravets, J. A. Grover, P. Solano, P. R. Kordell, J. D. Wong-Campos, L. A. Orozco, and S. L. Rolston, "Ultrahigh transmission optical nanofibers," AIP Adv. **4**(6), 067124 (2014).
36. R. E. Evans, A. Sipahigil, D. D. Sukachev, A. S. Zibrov, and M. D. Lukin, "Narrow-linewidth homogeneous optical emitters in diamond nanostructures via silicon ion implantation," Phys. Rev. Appl. **5**(4), 044010 (2016).
37. S. Pazzagli, P. Lombardi, D. Martella, M. Colautti, B. Tiribilli, F. S. Cataliotti, and C. Toninelli, "Self-Assembled Nanocrystals of Polycyclic Aromatic Hydrocarbons Show Photostable Single-Photon Emission," ACS Nano **12**(5), 4295–4303 (2018).
38. S. M. Skoff, D. Papencordt, H. Schauffert, B. C. Bayer, and A. Rauschenbeutel, "Optical-nanofiber-based interface for single molecules," Phys. Rev. A **97**(4), 043839 (2018).
39. R. C. Schofield, D. P. Bogusz, R. A. Hoggarth, S. Nur, K. D. Major, and A. S. Clark, "Polymer-encapsulated organic nanocrystals for single photon emission," Opt. Mater. Express **10**(7), 1586–1596 (2020).
40. T. T. Tran, M. Kianinia, M. Nguyen, S. Kim, Z.-Q. Xu, A. Kubanek, M. Toth, and I. Aharonovich, "Resonant Excitation of Quantum Emitters in Hexagonal Boron Nitride," ACS Photonics **5**(2), 295–300 (2018).
41. L. Spindlberger, A. Csóré, G. Thiering, S. Putz, R. Karhu, J. Hassan, N. Son, T. Fromherz, A. Gali, and M. Trupke, "Optical properties of vanadium in 4h silicon carbide for quantum technology," Phys. Rev. Appl. **12**(1), 014015 (2019).

Optics EXPRESS

42. A. Dietrich, M. W. Doherty, I. Aharonovich, and A. Kubanek, "Solid-state single photon source with Fourier transform limited lines at room temperature," Phys. Rev. B **101**(8), 081401 (2020).
43. M. Hoese, P. Reddy, A. Dietrich, M. K. Koch, K. G. Fehler, M. W. Doherty, and A. Kubanek, "Mechanical Decoupling of Quantum Emitters in Hexagonal Boron Nitride from Low-Energy Phonon Modes," arXiv:2004.10826 [cond-mat, physics:physics, physics:quant-ph] (2020).
44. J. Benedikter, H. Kaupp, T. Hümmer, Y. Liang, A. Bommer, C. Becher, A. Krueger, J. M. Smith, T. W. Hänsch, and D. Hunger, "Cavity-Enhanced Single-Photon Source Based on the Silicon-Vacancy Center in Diamond," Phys. Rev. Appl. **7**(2), 024031 (2017).
45. M. Pompili, S. L. N. Hermans, S. Baier, H. K. C. Beukers, P. C. Humphreys, R. N. Schouten, R. F. L. Vermeulen, M. J. Tiggelman, L. d. S. Martins, B. Dirkse, S. Wehner, and R. Hanson, "Realization of a multinode quantum network of remote solid-state qubits," Science **372**(6539), 259–264 (2021).
46. H. J. Kimble, "The quantum internet," Nature **453**(7198), 1023–1030 (2008).
47. N. Tomm, A. Javadi, N. O. Antoniadis, D. Najer, M. C. Löbl, A. R. Korsch, R. Schott, S. R. Valentin, A. D. Wieck, A. Ludwig, and R. J. Warburton, "A bright and fast source of coherent single photons," Nat. Nanotechnol. **16**(4), 399–403 (2021).
48. P. Steindl, H. Snijders, G. Westra, E. Hissink, K. Iakovlev, S. Polla, J. Frey, J. Norman, A. Gossard, J. Bowers, D. Bouwmeester, and W. Löffler, "Artificial Coherent States of Light by Multiphoton Interference in a Single-Photon Stream," Phys. Rev. Lett. **126**(14), 143601 (2021).
49. D. Awschalom, K. K. Berggren, H. Bernien, S. Bhave, L. D. Carr, P. Davids, S. E. Economou, D. Englund, A. Faraon, M. Fejer, S. Guha, M. V. Gustafsson, E. Hu, L. Jiang, J. Kim, B. Korzh, P. Kumar, P. G. Kwiat, M. Lončar, M. D. Lukin, D. A. Miller, C. Monroe, S. W. Nam, P. Narang, J. S. Orcutt, M. G. Raymer, A. H. Safavi-Naeini, M. Spiropulu, K. Srinivasan, S. Sun, J. Vučković, E. Waks, R. Walsworth, A. M. Weiner, and Z. Zhang, "Development of Quantum Interconnects (QuICs) for Next-Generation Information Technologies," PRX Quantum **2**(1), 017002 (2021).
50. T. Erdogan, "Fiber grating spectra," J. Lightwave Technol. **15**(8), 1277–1294 (1997).